IEEE Open Access Journal of Power and Energy

Received 29 December 2022; revised 3 June 2023 and 7 August 2023; accepted 4 September 2023. Date of publication 7 September 2023; date of current version 14 September 2023.

Digital Object Identifier 10.1109/OAJPE.2023.3312732

Evaluating the Precision of the DC Decay Test Method for Characterizing Wound-Field Synchronous Machines in Power Plants

FREDERIC MAURER[1], THOMAS ØYVANG[2] (Member, IEEE), AND JONAS KRISTIANSEN NØLAND[1,2] (Senior Member, IEEE)

[1]Department of Electric Energy (IEL), Norwegian University of Science and Technology (NTNU), 7034 Trondheim, Norway
[2]Department of Electrical Engineering, Information Technology and Cybernetics (EIK), University of South-Eastern Norway (USN), 3918 Porsgrunn, Norway

CORRESPONDING AUTHOR: J. K. Nøland (jonas.k.noland@ntnu.no)

This work was supported in part by the Research Council of Norway (RCN) under Grant 326673 (SysOpt Project).

ABSTRACT The sudden short-circuit test is the gold standard for determining the equivalent diagram of wound-field synchronous machines (WFSMs). Only a single measurement is needed while the machine is in saturated mode. However, this destructive test can significantly reduce the lifetime of the stator winding. Moreover, determining the equivalent diagram in the q-axis is more complicated and is often not performed. DC-decay tests are low-power alternatives that allow for the determination of the equivalent diagram in both axes without damaging the machinery. Until recently, they required the rotor to be aligned with the axes, which is not feasible in large power plants. A recent breakthrough eliminated the need for rotor alignment by proposing a DC-decay test that can be performed with the rotor in any position. However, numerous independent measurements are needed to obtain the equivalent diagram in both axes. This paper addresses the question of the minimum number of independent measurements needed for the DC-decay test to be practical for industrial use. Around 10 measurements are sufficient for reasonable precision, while 5 of high quality are sufficient using the symmetry of the root locus. Finally, a comparison against the short-circuit test shows that the DC-decay test is a valid alternative.

INDEX TERMS DC decay methods, parameter identification, pole estimation, equivalent diagrams, synchronous machines, current measurement, transient analysis, three-phase short-circuit.

NOMENCLATURE

T'_{d0}, T''_{d0}, T''_{q0}	Trans. & subtrans. open-circuit time const., $[s]$.
T'_d, T''_d, T''_q	Trans. & subtrans. short-circuit time const., $[s]$.
θ	Angle between rotor & stator phase a, $[rad]$.
$T_{\sigma D}$, $T_{\sigma f}$	Leakage time const. damper & field, $[s]$.
ω_n	Rated pulsation, $2\pi f_n$, $[rad/s]$.
x_{ad}, x_{aq}	Main d- and q-axis reactances, $[pu]$.
x_c	Characteristic reactance (Ref. [1]), $[pu]$ or $[\Omega]$.
x_d, x'_d, x''_d	Synchr., trans. & subtrans. d-axis react., $[pu]$.
x_q, x''_q	Synchr. and subtrans. q-axis reactances, $[pu]$.
i_a, i_b, i_c	Stator phase a, b and c current, $[pu]$ or $[A]$.
i_D, i_Q	Damper bar d- & q-axis current, $[pu]$ or $[A]$.
i_d, i_q	Stator armature d- & q-axis current, $[pu]$.
i_f	Rotor field winding current, $[pu]$ or $[A]$.
r_D, r_Q	Damper winding d- & q-axis resistance, $[pu]$.
r_s, r_f	Armature & field winding resistance, $[pu]$.
s	Laplace operator, $\frac{d}{dt}$, $[rad/s]$.
s_1, s_2, s_3, s_4	Poles of the armature transfer function, $[rad/s]$.
u_d, u_q	Stator armature d- & q-axis voltage, $[pu]$.

I. INTRODUCTION

TO BE able to analyze the transient behavior and dynamics of hydropower plants to ensure power system stability, a precise knowledge of the characteristic quantities of the wound-field synchronous machine (WFSM) is

required [2], [3], [4], [5], [6], [7]. Moreover, the estimation of the saturated sub-transient reactances x_d'' and x_q'' are essential for calculating the electrical and mechanical integrity of the machine and its shaft line during severe transients such as under three-phase or two-phase short-circuits. There are several methods available to obtain these quantities through normal procedures [8], where the DC decay method represents a non-conventional alternative [9]. In a DC decay test, the electrical machine has a locked rotor, with the rotor aligned with the direct or quadrature axis (i.e., (d- and q-axis) [10], [11], [12], [13], [14], [15], [16], [17], [18]. Then, DC current is injected in two phases of the machine armature (by closing SW_1 having SW_2 open), with a short-circuited field winding (see Fig. 1). After stationary conditions are achieved, the armature winding is then suddenly short-circuited with a circuit breaker (closing SW_2), and the decaying current (i_f and i_a or i_b) is recorded using a current probe. From these measurements, the parameters of the equivalent diagram are identified. This procedure requires less time, less power, and a significantly smaller short-circuit breaker than other methods, e.g., the three-phase short-circuit test. However, the DC decay method's most difficult part lies in the rotor alignment process with the d- or q-axis, which is very difficult to perform for large power plants. It is nearly impossible to align the rotor for big power units because of its huge weight to be turned manually. The large number of poles leads to a very high mechanical resolution, which is a complicating factor for rotor alignment. Consequently, rotor misalignment leads to a current response curve that is not pure, containing components of both axes, leading to inaccuracies in correctly computing the contribution of both axes. To enhance the applicability of the DC decay test, the rotor alignment challenge has to be solved, enabling simple techniques allowing for arbitrary rotor positions.

Earlier works assumed the rotor to be aligned with the d- or q-axis, or provide a procedure to align it [10], [11], [12], [13], [14], [15], [16], [17], [18], which is nearly impossible to achieve for large power units. However, recent contributions take another path to simplify the measurements, allowing for arbitrary rotor positions [19], [20], [21]. Nevertheless, they lack direct comparison against the sudden short-circuit test nor provide any complete precision sensitivity analysis in the case of a practical power application. Other contributions analyze other aspects of these approaches. The equivalent diagram of parameters has been identified using low-pass functions [10]. A fast Fourier transform (FFT) was applied to the time signals [11], [15]. It was also applied in the stand-still frequency response (SSFR) tests [22]. The characteristic quantities can also be estimated by curve-fitting techniques of the measured decay current, where the poles and zeros of the transfer function are identified, which indirectly reveals the characteristic quantities [11], [16]. Genetic algorithms have also been introduced on this matter [13]. Moreover, a combination of genetic and Gauss-Newton algorithms has been used for parameter estimation [14]. By minimizing an objective function using Levenberg-Marquardt's algorithm,

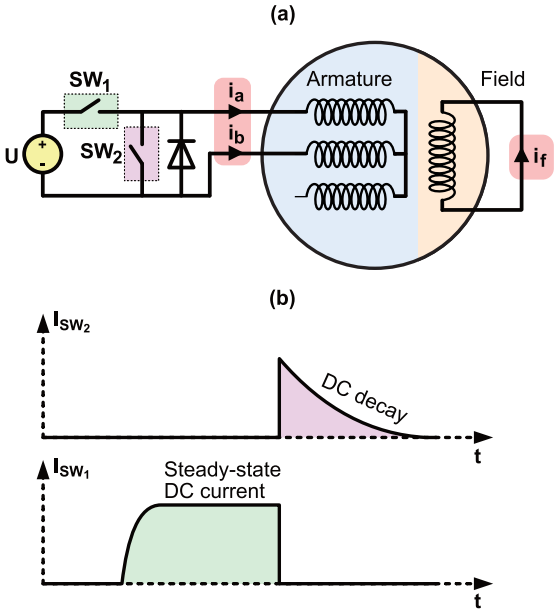

FIGURE 1. (a): Experimental test scheme for the DC decay method for SM2. (b): Current through the DC-decay switches, adapted from [20].

one can also determine the characteristic quantities [17], [18]. A method to obtain the characteristic quantities for any rotor position was proposed decades ago [23]. Similar approaches have been proposed more recently [11], [16]. However, the drawback is that the modeling of the short-circuit is not precise enough to avoid discrepancies appearing between the identified parameters and the theoretical ones.

Based on the above motivations, this paper presents a simulation study that extends the method described in [20] to analyze the optimal number of measurements and recordings for a real-world power plant application. The objective is to figure out the minimum number of recordings required to obtain an equivalent diagram with a given precision. Moreover, the equivalent diagram of a laboratory WFSM is measured and validated through simulation. Our work is then compared with what is obtained through a three-phase short-circuit test to provide a reference point and increase confidence in the proposed method. The paper also discusses the practicality of different equivalent diagrams and considers the maximum exerted torque of the WFSM, though it does not address the dynamic speed response due to the assumption of high inertia.

The paper is organized with the following structure. Section II recalls and briefly adapts the main mathematical expressions, identification algorithms and measuring methods developed in [20] and [24]. Then, Section III presents the results of a parameter identification robustness study simulating the machine SM1. This is a high-power WFSM with known design values and parameters provided in Tables 1 and 2, with well-established and measured characteristics prior to this paper [20]. The experimental results are presented in Section IV, which also provides a

TABLE 1. Synchronous machine's rated data - SM1 & SM2.

Symbol	Quantity	SM1	SM2
S	apparent power	180.0 MVA	2.3 kVA
U_s	stator voltage	13.8 kV	380 V
I_{f0}	no-load field current	1050.0 A	2.0 A
n	mechanical speed	150 r/min	1500 r/min
f_s	stator frequency	50 Hz	50 Hz

comparison against the sudden short-circuit test. Measurements are extracted from machine SM2, which is the highest-power WFSM available at the laboratory used during this work. Tables 1 and 8 provide ratings and measured parameters.[1] Finally, Section V concludes the paper and discusses future research items.

II. THEORETICAL BACKGROUND OF DC DECAY

Starting from the voltage equations for u_a and u_b, presented in [25], with $i_c = 0$ and $i_b = -i_a$, one can obtain the transfer function for the test circuit presented in Fig. 1-(a). This transfer function considers one damper circuit per axis, corresponding to the modeling of large WFSMs with laminated salient poles with a copper bar damper windings [26].[2] Herein, U is the voltage of the DC voltage source utilized in the experiment, which drives a measurable stator current i_a. In order to obtain the characteristic reactance x_c, the field current (i_f) is also recorded (as indicated). SW_1 and SW_2 are the switches used for this test. Incorporating the characteristic reactance is fundamental to correctly computing the transient excitation current, but it has no impact on the stator current computation. Hence, it is often overlooked in WFSM characterization.

To perform the test (refer to Fig. 1), first, SW_1 is closed while SW_2 remains open, enabling a DC-current to flow in the armature winding. After reaching a steady current, switch SW_2 is closed and SW_1 is opened at the same time. This way of handling the switches is shown in Fig. 1-(b). The decay of the stator current is then recorded using a transient recorder. Opening SW_1 is only necessary to protect the DC voltage source from any damages. Finally, when the armature current is zero, SW_2 can be opened.

The transfer function of the setup described in Fig. 1, assumes small variations, given by [20]

$$i_a(s) = -i_b(s) = \frac{Y_f(s)Y_Q(s)}{Y_{ab}(s)} u_{ab}(s), \tag{1}$$

where $Y_{ab}(s)$ is defined as

$$Y_{ab}(s) = 2\left[r_s + \frac{1}{3}s\left(\alpha^2\frac{x_d}{\omega_n} + \beta^2\frac{x_q}{\omega_n}\right)\right] Y_f(s)Y_Q(s) - Y_Q(p)\frac{2}{3}\frac{\alpha^2 x_{ad}^2}{\omega_n^2}\left(\frac{1+sT_{\sigma D}}{r_f} + \frac{1+sT_{\sigma f}}{r_D}\right)s^2$$

[1]No design values are available for this machine.

[2]This type of machine has been handpicked, as it represents more than 95 % of the installed power generation facilities in hydropower.

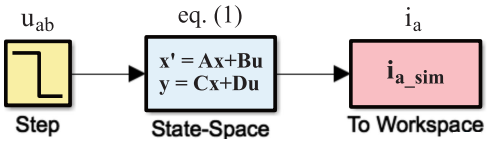

FIGURE 2. MATLAB state-space simulation model. Adopted from [20].

$$- Y_f(s)\frac{2}{3}\frac{\beta^2 x_{aq}^2}{r_Q\omega_n^2}s^2, \tag{2}$$

with $\alpha = \cos(\theta) - \cos(\theta - \frac{2\pi}{3})$ and $\beta = \sin(\theta) - \sin(\theta - \frac{2\pi}{3})$. Moreover, the polynomials $Y_f(s)$ and $Y_Q(s)$ are expressed as

$$Y_f(s) = (1 + sT'_{d0})(1 + sT''_{d0}), \quad \text{and} \tag{3}$$
$$Y_Q(s) = 1 + sT''_{q0}. \tag{4}$$

Eq. (1) has identifiable poles found in eq. (2), yielding

$$Y_{ab}(s) \propto (s + s_1)(s + s_2)(s + s_3)(s + s_4). \tag{5}$$

The non-linear coupling between the two axes is described by eq. (1) for $Y_{ab}(s)$, using the constants α and β. To obtain the equivalent circuit for both axes, we must consider the angular variation ("root-locus") of the four zeros of $Y_{ab}(s)$ (s_1, s_2, s_3, and s_4), as described in eq. (5). This root-locus exhibits four minima and four maxima, which correspond to a zero or pole of the transfer functions in the d- or q-axis, as explained in reference [24]. From these poles and zeros, we can deduce the equivalent diagram. However, the transfer function for a machine oriented with only one axis has fewer poles and zeros than the transfer function described in eq. (1). Thus, it can complicate the estimation of the minima and maxima of the root-locus and affect the identified characteristic quantities, as discussed in Section III. The parameter identification algorithm follows the steps outlined in [20], including techniques for removing outliers and improving the algorithm's precision.

The determination of x_c is done using a similar procedure as presented in [1]. The transfer function between the d-axis armature current and the field current is given by

$$i_f(s) = -\frac{sx_{ad}(1 + sT_{\sigma D})}{r_f\omega_n(1 + T'_{d0})(1 + T''_{d0})} i_d(s). \tag{6}$$

The time constant $T_{\sigma D}$ is identified using i_f. By assuming a certain value of x_c, the equivalent circuit is computed using the identified characteristic quantities, where $T_{\sigma D}$ is computed from the equivalent circuit. If the error between the identified $T_{\sigma D}$ and the computed one is less than a given threshold, then the assumed value of x_c is correct. If the error is too high, then the assumed value of x_c is increased by a given step, and the procedure is repeated up to convergence.

III. PARAMETER IDENTIFICATION ROBUSTNESS STUDY

In order to gain new insight into the sensitivity of the DC decay method, a robustness study was carried out in the

TABLE 2. Reference standard parameter values for synchronous machine SM1.

x_d	x'_d	x''_d	x_q	x''_q	x_c	T'_{do}	T''_{do}	T'_d	T''_d	T''_{qo}	T''_q
1.0250 pu	0.2960 pu	0.1980 pu	0.7090 pu	0.2020 pu	0.1150 pu	8.9095 s	0.0417 s	2.5630 s	0.0280 s	0.1088 s	0.0310 s

simulation-based environment for machine SM1. The simulation setup in the MATLAB/Simulink environment is shown in Fig.2. The transfer function of eq. (1) was used for the machine SM1, with parameters specified in Table 2. Results are obtained assuming ideal switches, switching simultaneously, with no transition time. All the equations are linear, with the voltage source element having a constant voltage. The steady-state current (i_a) is 100 A and the voltage step in u_{ab} is 0.529 V (i.e., corresponding to 100 A). The transfer function was formulated and calculated using a state-space representation. All simulations were performed with the same initial conditions. The rotor angle and sampling frequency were adjusted as input parameters to meet the goals of this study. White noise was modeled using the ad hoc element in the MATLAB environment. The basic principle behind this study is to start with machine parameters that are assumed to be well known and try to replicate them again with some errors to be analyzed under various conditions. Hence, we mimic the measurement conditions in a real-world power plant.

The sensitivity of recording was studied in the MATLAB environment, varying the sampling frequency from 1 kHz to 5 kHz. Fig. 3 show the influence of the sampling period on the point-by-point capturing of four poles as a function of rotor angle. The exact values of the poles to be identified are detailed in Table 3. A variation of the sampling frequency between 1 kHz and 5 kHz[3] induces a variation of the radius of convergence of the identification algorithm, which was about 10 ° for the s_1 pole, 5 ° for the s_2 pole, 3 ° for the s_3 pole and 5 ° for the s_4 pole. The sampling frequency of 1 kHz creates new identification errors, e.g., for angles of 150 ° and 330 ° for the s_2 pole. This effect is related to the number of samples available to converge the non-linear algorithm so that a too-small sampling frequency should be avoided.

The errors are the highest for electrical angles in the region around 60 °, 150 °, 240 °, or 330 °. This effect is related to the pole/zero simplification, which prevents the convergence of the curve fit algorithm. These regions, where the error is large, remain visible when the sampling frequency is varied. The error increase is important for the s_2 pole, which can induce an error when obtaining the maxima and minima of this pole. The error is highest with the lowest sampling rate (1 kHz). However, the value of the error is not identical for all poles. The maximum value of the error is about 10 % for the s_1 pole, approximately 50 % for the s_2 pole, while it is less than 1 % for the s_3 pole, and finally, less than 0.2 % for the s_4 pole.

[3]This frequency swipe have been chosen as it represents a "classical" frequency range of transient recorder used in high power machines. In addition, several simulations showed that increasing the sampling frequency doesn't improve the identification quality especially when adding noise.

TABLE 3. Obtained poles of sm1 from Tab. 2 values using Eqs. (2)-(5).

Pole	Minima	Maxima	Mean
$s_1(\theta)$	−37.1292 rad/s	−35.1303 rad/s	−36.3109 rad/s
$s_2(\theta)$	−23.9775 rad/s	−9.1961 rad/s	−16.6623 rad/s
$s_3(\theta)$	−2.8386 rad/s	−1.0174 rad/s	−1.6916 rad/s
$s_4(\theta)$	−0.1122 rad/s	−0.1012 rad/s	−0.1065 rad/s

TABLE 4. Pole estimation's root mean square error as functions of sampling time and frequency with data given in Fig. 3.

T_s / f_s	$s_1^*(\theta)$	$s_2^*(\theta)$	$s_3^*(\theta)$	$s_4^*(\theta)$
0.2 ms / 5.00 kHz	0.41535	2.86104	0.00152	0.00002
0.3 ms / 3.33 kHz	3.74464	3.72127	0.10771	0.01188
0.4 ms / 2.50 kHz	3.74588	3.72658	0.10771	0.01188
1.0 ms / 1.00 kHz	3.77047	4.05882	0.10776	0.01188

The higher the sampling frequency, the smaller the error, which can be clearly seen in the root mean square errors (RMSEs) given in Table 4.

Another important characteristic of the DC decay is the influence of the number of measurements, i.e. the number of short circuits to be performed over 360 °, on the identification of the maxima / minima of the poles. The angular pitch was varied according to the following list: 1 ° (360 test), 2 ° (180 tests), 5 ° (72 tests), 10 ° (36 tests), 15 ° (24 tests), and 20 ° (18 tests), 25 ° (14 tests) and 30 ° (12 tests). In order to determine the minimum and maximum values of the poles, we need to consider not only the number of tests but also the harmonic content of the fitting function. Table 5 displays the 13 cases we studied for the variation of the harmonic content. It is worth noting that adding odd harmonics to the Fourier series approximation of the poles, such as s_1 is formulated in (7), does not have any physical meaning, other than potentially aiding the curve fit algorithm in its convergence.

$$s_1(\theta) \approx \frac{a_0}{2} + \sum_{k=1}^{n} a_n \cos(n\theta) + \sum_{k=1}^{n} b_n \sin(n\theta), \qquad (7)$$

Fig. 4 shows the effect of varying the harmonic content and the number of measurements on the error identifying the maxima/minima of the poles. In particular, for the angular steps of 25 ° and 30 °, the method does not reliably identify values from the curves given by the curve fit approach. Interestingly, in most cases, an increase in harmonic content leads to a reduction in the identification error. This error fluctuates but converges towards a certain value (s_1 and s_3 pole curves). In almost all cases, adding odd harmonics to the curve fit does

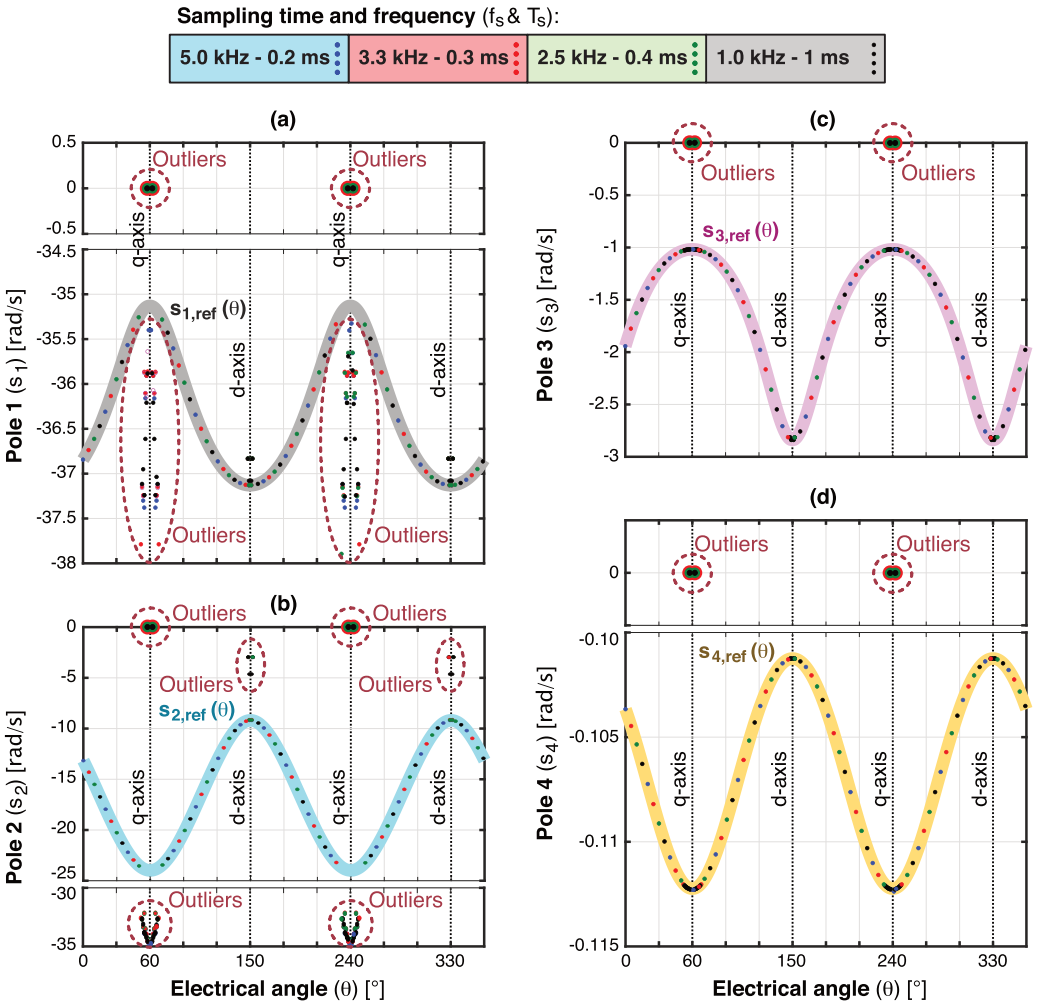

FIGURE 3. **Influence of the sampling time on the identification of the poles for machine SM1. (a): s_1; (b): s_2; (c): s_3; (d): s_4. Error analysis given in Table 4.**

TABLE 5. **13 cases of harmonic content for fitting function in Eq. (7).**

Case number	Even harmonics	Odd harmonics
#1	$k = 2, 4$	-
#2	$k = 2, 4, 6$	-
#3	$k = 2, 4, 6$	$k = 1$
#4	$k = 2, 4, 6$	$k = 1,3$
#5	$k = 2, 4, 6, 8$	-
#6	$k = 2, 4, 6, 8$	$k = 1$
#7	$k = 2, 4, 6, 8$	$k = 1, 3$
#8	$k = 2, 4, 6, 8, 10$	-
#9	$k = 2, 4, 6, 8, 10$	$k = 1$
#10	$k = 2, 4, 6, 8, 10$	$k = 1, 3$
#11	$k = 2, 4, 6, 8, 10, 12$	-
#12	$k = 2, 4, 6, 8, 10, 12$	$k = 1$
#13	$k = 2, 4, 6, 8, 10, 12$	$k = 1, 3$

not improve the result. Consequently, the addition of these harmonics is not necessary.

In the case of the minimum value of the s_4 pole, increasing the harmonic content increases the error. Although the absolute value of the error is almost zero, it should be remembered that the most probable solution is not necessarily the one with the highest case number. It is, therefore, necessary to check which curve fit gives the most probable value. The identification error is maximal for the s_3 pole, and it is about 100 times less for the s_4 pole. The identification of the maximum and minimum of the s_3 pole has a maximum error because the curve showing the variation of the pole as a function of electrical angle does not have a sinusoidal trace. In general, the error is not of the same order of magnitude for all four poles. The maximum error is 0.25 % for the s_1 pole, 1.4 % for the s_2 pole, 4.5 % for the s_3 pole, and 0.05 % for the s_4 pole.

In addition to the analysis above, two additional effects have been studied. One is the effect of a non-constant angular pitch, and the other is the effect of a parity propagation of the measurement points. These two additional effects only have a practical meaning, reducing and simplifying the measurements. The non-constant angular step does not lead to any notable difference compared to the results in Fig. 4. The errors fall within the limits of the Fig. 4. This effect

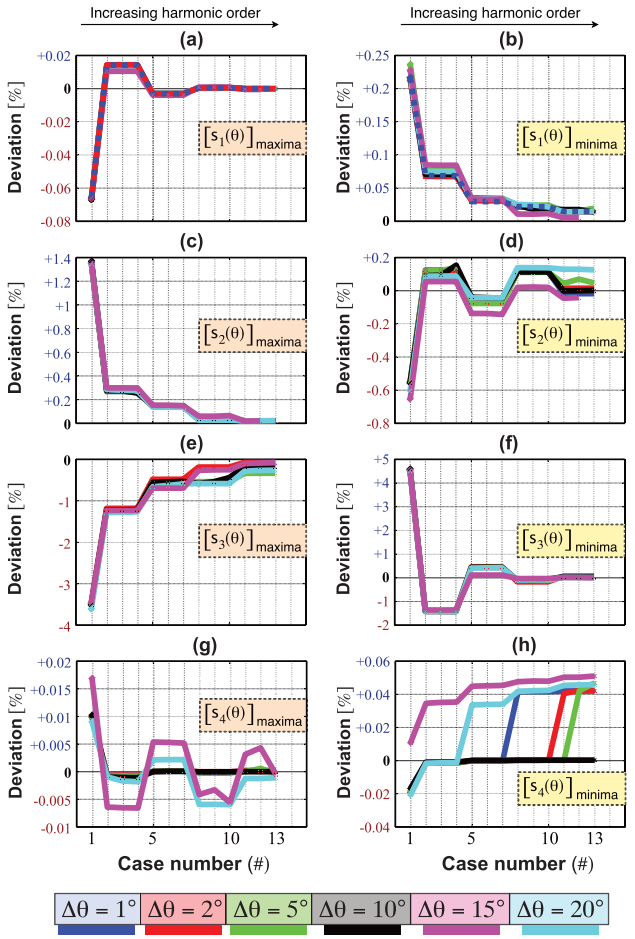

FIGURE 4. Effect of a variation of the harmonic content on the identification error of the maxima / minima values of the poles for the SM1 machine for a sampling period of 0.2 ms (reference values given in Table 3). Increasing case number means increasing harmonic content, as described in Table 5. The deviation is given in % of the minima and maxima defined in Table 3. As an example, the reference value for subfigure a) is -37.1292 rad/s. The colors of the curves refers to the angular step ($\Delta\theta$), as depicted inside figure. (a): Maxima $s_1(\theta)$; (b): Minima $s_2(\theta)$; (c): Maxima $s_1(\theta)$; (d): Minima $s_2(\theta)$; (e): Maxima $s_3(\theta)$; (f): Minima $s_3(\theta)$; (g): Maxima $s_4(\theta)$; (h): Minima $s_4(\theta)$.

was studied for an angular step of 15 °+5 °[4] and for a sampling period of 0.2 ms. The second additional effect is the propagation of measurement points. This involves making, for example, a number of measurements between 60 ° and 150 ° and using the symmetries present in the variation of the poles to deduce all the other values. This technique requires the angle θ to be known absolutely [20]. However, it has the disadvantage of propagating the errors of identification of the poles. On the other hand, it introduces perfect symmetries, which can also improve the convergence of the curve fit algorithm. A test was performed for an angular step size of 1 ° and a sampling period of 0.2 ms. No significant differences could be found. The errors fall within the limits of the Fig. 4.

To study the effect of the signal-to-noise ratio (SNR) on the identification of the equivalent diagram, two sets of simulations were conducted using MATLAB. Gaussian white noise was added to the simulated stator current to create an SNR of 40 dB in the first set of simulations and an SNR of 60 dB in the second set. The major impact of the noise lies on the poles s_2 and s_3. The other two are quasi-unaffected by the noise. Reducing the angular step below 10 ° helps to keep the identification error below 1 %, but they can also induce biased poles near the axis. One should therefore keep the distance. Approximately 5 ° is sufficient along the axis during the measurements to avoid the biased poles that are difficult to remove using the algorithm developed in [20] and [24]. Another option would be to increase the robustness of the algorithm in this region, which could be the subject of further research.

Table 1 in reference [20] presents the results of the identification of characteristic quantities by simulation for the SM1 machine. These results presented show the minimum and maximum errors obtained. The simulations, separately validated using SIMSEN [27], were performed with a system of state equations written in MATLAB. It can be concluded from the robustness study that the maximum error is less than 1 %, which verifies the quality and accuracy of the identification method. It can also be seen that a sampling period of 1 ms causes an offset on the error. All the errors for a sampling period of 1ms are greater than those for a sampling period of 0.2 ms.

Fig. 5 show the effect of a variation in the number of measurement points and a variation in the sampling period on the characteristic standard quantities of the SM1 machine. The error is relative to the parameters given in Table 2. For each angular step, the maximum and minimum values of the poles chosen are those with the lowest error. Therefore, these are results in the best case. It can be seen that the errors are always less than 1 %, highlighting the precision of the method and the very limited impact of sampling frequency and number of measurement on the obtained characteristic quantities. This also means that for a high power unit, there will be no impact coming from sampling frequency or number of measurements on the results in the best case.

In general, the value of the errors does not vary in the same way for all the characteristic quantities. The maximum errors are obtained with high angular steps (few recordings). Therefore, in order to keep the deviation within reasonable limits, no angular step greater than 10 ° should be chosen (i.e., less is better, and symmetries can be used to exploit each measurement better). The sampling period does not influence the error uniformly. However, a trend, saying that a low sampling period guarantees a low error, seems to emerge anyway. The non-linear influence of the studied parameters does not allow to draw uni-vocal conclusions. By keeping the signal-to-noise ratio above 40 dB guarantees a good identification quality.

[4]The variation of the angular step was carried out using pseudo-random values uniformly distributed between 0 and 5.

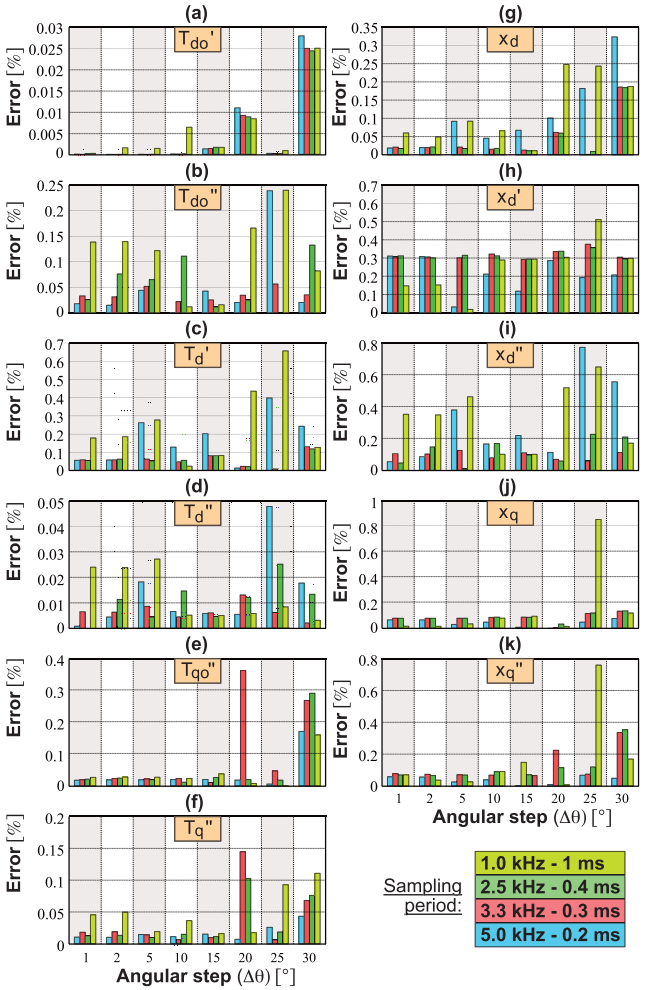

FIGURE 5. Effects of a variation in the number of measurement points (i.e., angular step, $\Delta\theta$) and a variation in the sampling period (T_e) on the characteristic quantities of the direct axis of the SM1 machine. (a): T'_{do}; (b): T''_{do}; (c): T'_{d}; (d): T''_{d}; (e): T''_{qo}; (f): T''_{q}; (g): x_d; (h): x'_d; (i): x''_d; (j): x_q; (k): x''_q. The error is relative to the parameters given in Table 2.

IV. EXPERIMENTAL RESULTS

In this section, explicit validations to the numerical analysis are provided. For this reason, the experimental setup is depicted in Fig. 6 while Fig. 1 shows a schematic layout of the DC decay method, as proposed in [10] and using the measurement methods described in Section I.

As the bearings of the machine are always lubricated, one needs a shaft-blocking device to prevent any rotor movement during the measurements (as indicated in Fig. 6). This device can be very rudimentary, as the torque occurring during these tests is very small. For the DC decay method, the maximal value of the torque (T_{max}) achieved during the steady-state condition prior to the decay process is given by

$$T_{max} = \frac{4}{9} I_a^2 \alpha\beta (x_d - x_q) \cong 0.3 I_a^2 (x_d - x_q), \qquad (8)$$

where I_a is the stationary pu-value of the stator current.

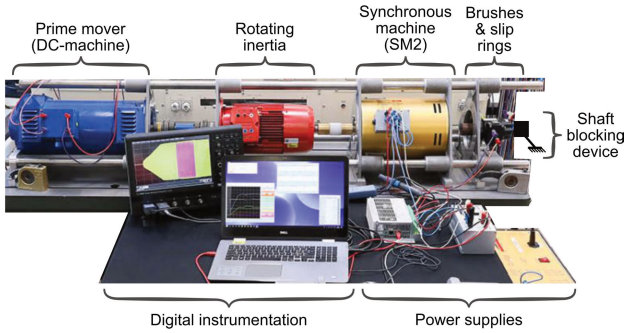

FIGURE 6. Experimental setup for the 2.3-kVA, 380-V, 1500-rpm synchronous machine SM2, with nominal data given in Table 1, test setup specifications provided in Table 6, and identified standard parameter values listed in Table 8.

TABLE 6. Specification of the experimental test setup for machine SM2.

Description	Value
Rated power factor of the synchronous machine (SM2)	0.80
Rated AC current of the synchronous machine (SM2)	3.50 A
Rated DC voltage for SM2 excitation via slip rings	24.00 V
Rated DC current for SM2 excitation via slip rings	4.50 A
Rated mechanical power of the DC machine	1.84 kW
Rated mechanical speed of the DC machine	1.50 krpm
Rated mechanical torque of the DC machine	11.71 Nm
Rotating inertia installed on the shaft	0.34 kgm^2

TABLE 7. Alternative methods to obtain the parameters of the equivalent diagram.

Parameters	Method / Norm
x_d	Permanent short-circuit mode
x'_d, x''_d	Three-phase short-circuit / application of voltage
T'_d, T''_d	Three-phase short-circuit
x_q	Negative excitation
x''_q	Application of voltage
T''_q	Three-phase short-circuit in operation
x_c	Three-phase short-circuit (excitation current)

SM2 depicted in Fig. 6 is a salient-pole machine with the highest output power available at the laboratory facilities having laminated salient poles. A laminated salient pole (i.e., SM1 and SM2) is composed of stacked and already cut iron sheets to form the desired pole shoe shape pressed together with clamping bolts and has a copper damper winding.

In order to sufficiently determine the equivalent circuit for both axes, one usually needs to perform between 10 and 20 measurement processes with a rotor displacement of 180 ° between the first and the last recording. As a reference to the parameters obtained via the DC decay method, one can use methods coming from norms (IEEE, IEC). Table 7 presents the method and norm used to determine the standard parameters using alternative methods, which have earlier been applied to SM2 for the equivalent diagram's parameters.

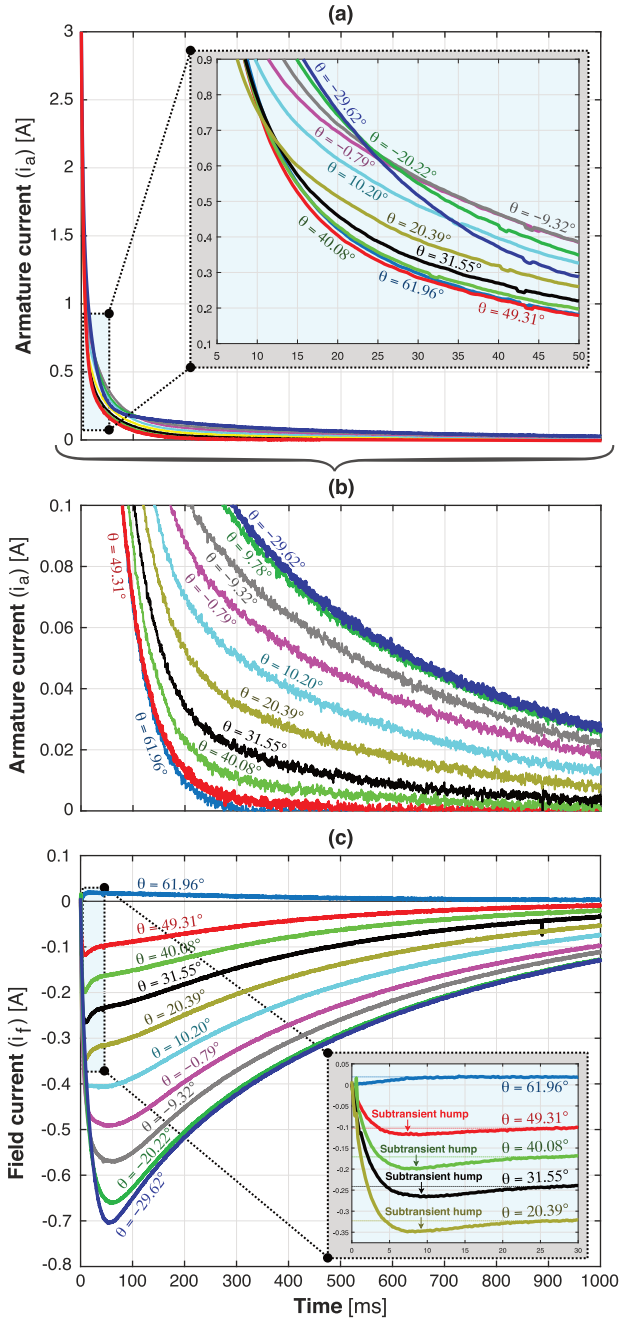

FIGURE 7. **Measured stator armature current (i_a) and rotor field current (i_f) for different rotor positions in the machine SM2, where stator d- and q-axis are located at $\theta \approx 150$ ° and $\theta \approx 60$ °, respectively. The initial armature DC current level was set to $i_a \approx$ -3.0 A and $i_b \approx 3.0$ A at 0 ms, while $i_c = 0$ A during the whole time interval. The initial field current (i_f) was 0 A at 0 ms. (a): i_a plots in full view. (b): i_a plots in zoomed view. (c): i_f plots.**

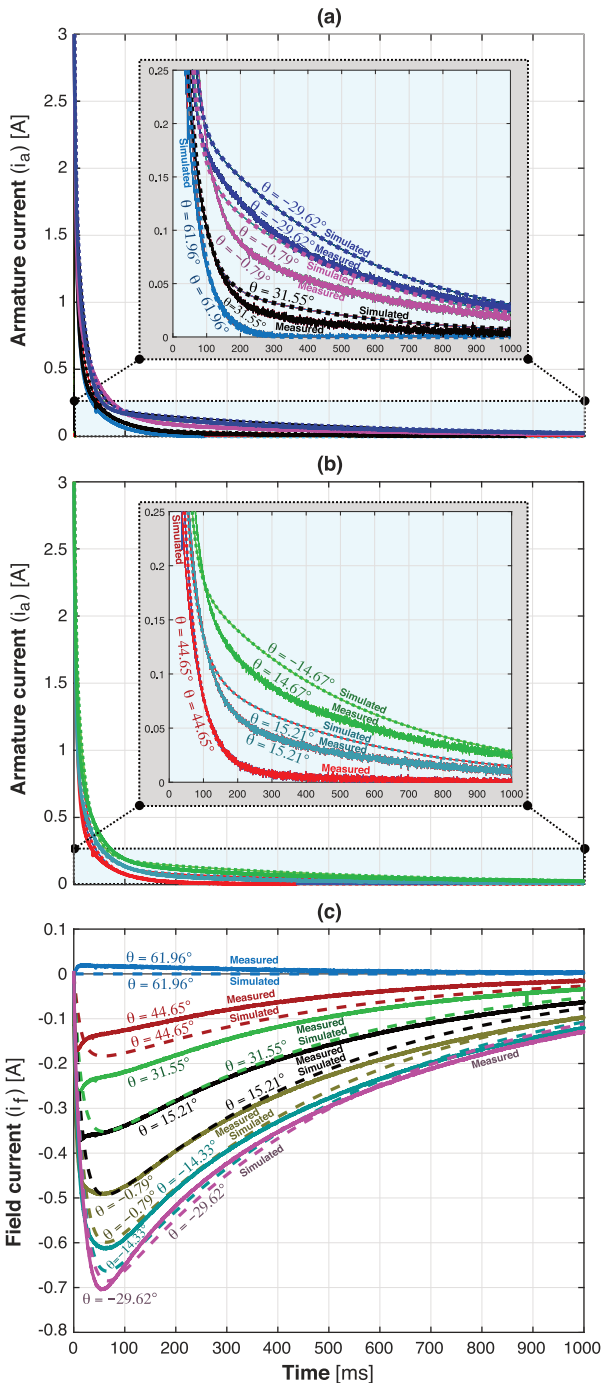

FIGURE 8. **Comparison between handpicked measured sequences from Fig. 7 against simulated profiles in the SIMSEN numerical environment. (a) & (b): Stator armature current (i_a). (c): Rotor field current (i_f).**

A. RECORDINGS OF THE DC DECAY TEST

A total of 38 tests were conducted at different rotor angles, covering an angular range of approximately 180 °. Fig. 7 depicts the time evolution of the stator current decay of the SM2 machine during the DC decay test. The shift in response from the d-axis to the q-axis shows peculiar behavior. Instead of having one slip zone, the curves in Fig. 7 show two quite distinct zones, one for positions approaching the d-axis and the other for positions in the region around the q-axis. This effect could be explained by the fact that SM2 is a low-power machine and has a huge saliency effect due to its very narrow air-gap (i.e., 3 mm).[5] The evolution of the sub-transient

[5]This high saliency effect makes that the fundamental theory underpinning the equivalent diagram less precise.

TABLE 8. Identified standard parameters of SM2 using the DC decay tests obtained from Fig. 6 and the short-circuit test in Fig. 8.

Test method	x_d	x'_d	x''_d	x_q	x''_q	T'_d	T''_d	T''_q
DC decay test	0.7842 pu	0.2541 pu	0.1089 pu	0.2325 pu	0.1069 pu	147.2 ms	4.7 ms	17.7 ms
Three-phase SC test (from [28], 1 pu)	1.0810 pu	0.1665 pu	0.0800 pu	0.2600 pu	0.0800 pu	29.5 ms	9.6 ms	7.7 ms
Three-phase SC test (from [28], 0.2 pu)	1.2756 pu	0.2089 pu	0.1205 pu	n/a	0.1205 pu	51.8 ms	10.7 ms	n/a

quantities more or less corresponds to the evolution of the sub-transient quantities of the SM1 machine with a time constant of the d-axis lower than that of the q-axis. Note that the response of the d-axis for rotor angle -29.62 ° is peculiar for the small experimental machine, which has a short, concentric air gap of 1-2 mm length. Fig. 7 also shows the time evolution of the rotor field current, as the exciter terminals are short-circuited. For rotor angles between 40 ° and 60 °, the response has a hump in the sub-transient part of the response, which can not be described using the classical equivalent diagram for WFSMs. This hump can be attributed to the same as the above-mentioned reasons.

Due to the observed large saliency effect, the procedure to determine the equivalent diagram had to be adjusted. After several attempts to use the four-pole transfer function, the approach did not succeed in the entire region. Therefore, near the d-axis, identification was conducted using a three-pole transfer function, while two poles were used near the q-axis. Using these root locus's, one can determine its maximum and minimum as usual from which the equivalent diagram can be computed.

B. ASSESSMENT OF MEASUREMENTS AGAINST SIMULATIONS

The recorded current decays are used to uncover the limits of simulations using the equivalent diagram in this subsection, and especially considering low-power WFSMs. Using simulations done in the SIMSEN numerical environment, we compare the simulated curves based on the base quantities of SM2 in Table 1 and its standard parameters in Table 8 with measured currents. When the machine is aligned with the d-axis, the difference between simulated and measured armature current is relatively low, revealing the high accuracy of the developed method in this study. The measured curves do not exactly represent the curves in the d- and q-axis; however, the angular deviation is assumed to be small enough to verify the numerical basis for this work.

Fig. 8 show the comparison between simulated and measured currents for angles ranging from 0 ° to 90 °. The correspondence is excellent for angles in the vicinity of the d- and q-axis. On the other hand, the deviation is more important for angles ranging from 15 ° to 45 ° because we change the slip zone. These slip zones were not being modeled by the identified machine model. Fig. 8 also shows a comparison between the measured and simulated curves for i_f. The deviation is greater than that obtained for the stator current. Nevertheless, the agreement between the curves remains satisfactory, especially for the estimation of the maximum value reached by the current. However, it can be seen that the error varies strongly with the electrical angle. Similarly, the estimation of the maximum current value shows errors of the order of 20 %. Moreover, the hump observed in the sub-transient part of the response for angles of about 60 ° to 80 ° is not modeled by the classical equivalent diagram.

Overall, the results are good from a validation point of view. The comparison between the simulation and the measurement showed an excellent agreement between the simulated curves and the measured curves when the machine is shimmed in one of the 2 axes. In between, the agreement is more or less good, as the model used does not perfectly translate the physical reality of this low-power machine. On the other hand, the error in the excitation current is greater but still acceptable for the purpose of machine characterization.

C. ALTERNATIVES FOR DETERMINATION OF THE EQUIVALENT CIRCUIT

Table 8 compares the obtained equivalent diagram for the DC decay test, and the classical three-phase short-circuit test, respectively. It is very important to note that, as one can see in Figs. 8 and 9, each method has a very good agreement between measurement and simulation for their respective identified parameters. For the DC decay method, most parameters identified for the d-axis (e.g., x_d, x''_d, T'_d, and T''_d) are perceived as the most accurate, given the nature of the method and the fact that SM2 is a low-power machine with laminated salient poles. However, the value of x_d is very high, and x_q is very low compared to typical values expected for salient pole machines. These values might be affected due to the signal-to-noise ratio (SNR) at the measurement level is too low in the time interval where these quantities are determined. This condition must be studied with further measurements on a high power machine in a power plant.

For the short-circuit test, the time constants are perceived to be very low compared to "classical values". Given the measurements, it is difficult to compute them with precision, i.e., the results should be taken with a certain precaution. For example, considering the very low value of the sub-transient time constant (T'_d), the use of the standardized classical method should be questioned on this basis. In fact, the conventional approaches lead to only a few data points, causing their identified values to be inversely proportional to the voltage, which is the main drawback of the three-phase SC test for low-power machines.

Fig. 9 presents a comparison between the two parameter sets outlined in Table 8, focusing on their predictive capabilities for sudden short-circuit (SC) occurrences at rated voltage. Notably, the three-phase SC test exhibits superior precision for this specific scenario. While the disparity in current peak

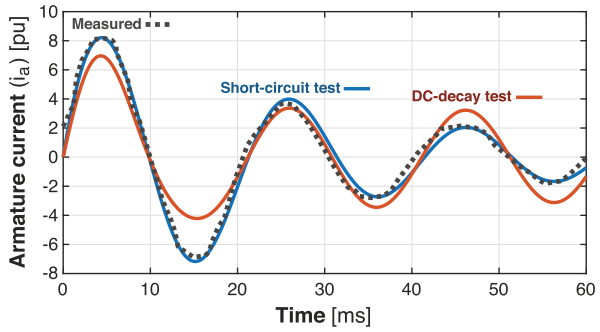

FIGURE 9. Armature current response of a sudden three-phase short-circuit at rated voltage (380 V**) and frequency (**50 Hz**), with** 2.02 A **field current and** 1500 r/min **mechanical speed, comparison measurement against simulations using the parameters from the short-circuit test and the DC decay test (given in Table 8), respectively. Measurements taken from the technical report of Wymann et al. [28] for the same machine SM2. The base value of the armature current is** 3.5 A**.**

values hovers around 20 %, it remains within the permissible tolerances set forth by IEC/IEEE standards. It is worth noting that the DC decay value struggles to replicate the short-circuit test at rated voltage, particularly during the initial stages of saturation. A likely cause for this discrepancy is attributed to the erroneous x_d value, prompted by extremely low SNR and that the DC decay test cannot saturate the machine as the short-circuit test. It is also worth noting that the parameters derived from our analysis fall outside the conventional range, aligning with expectations for smaller machines [29], [30]. The significance of the 20 % error margin should be interpreted within the context of low-power machines, which are susceptible to a more pronounced saliency effect arising from their relatively small air gap. As a result, the fundamental theory underlying the equivalent diagram tend to be less accurate compared to high-power machines with larger air gaps.

The obtained parameters were consistent with those obtained under non-saturated conditions (0.2 pu of rated voltage - Table 8). It confirms that the DC decay test is a reliable method for determining the equivalent diagram of a WFSM. In addition, the maximum torque amplitude during the DC decay test was in the range of 0.2 pu, while it reached 8 pu for the sudden short-circuit at rated voltage, i.e., 16 times the value of the DC decay test. This is a significant advantage, as the DC decay test performs at least as well as the sudden short-circuit but without the risk of damaging the machine or reducing its lifespan. As a result, the DC decay test can be conducted without any restrictions.

V. CONCLUSION

This paper presents the main challenges in performing DC decay tests on wound field synchronous machines (WFSMs). It includes a comprehensive sensitivity analysis of sampling frequency and angular resolution. We show thoroughly that these factors can significantly impact the identification of the equivalent diagram and the susceptibility to measurement noise. As noted in previous research [20], the DC decay method has a disadvantage in obtaining x_d and x_q due to the low signal-to-noise ratio (SNR) in the time interval where these values are obtained.

The identification algorithm's robustness was demonstrated under non-ideal conditions, and there was good agreement between simulation and measurement in the identification of the equivalent diagram of a low-power WFSM. However, it is widely accepted that the classical equivalent diagram has limitations for smaller machines. To achieve an identification precision below 1 %, we recommend an SNR above 40 dB, a sampling frequency at 5 kHz, and an angular resolution below 10 ° with measurement propagation. A minimum of 9 recordings should be sufficient, while 10 to 12 tests would be even more accurate.

A comparison was also conducted between a short-circuit test and a DC decay test, using data measured at rated voltage. To the best of our knowledge, this is the first attempt at such a comparison. We found that the DC decay test falls within the accepted 20 % current error as per IEC/IEEE standards, even in the saturated case for a small power machine where it is known that parameters do not behave normally. Comparison with non-saturated values also resulted in an acceptable discrepancy. The maximum torque amplitude was reduced by a factor of 16 compared to the gold standard, i.e., the sudden short-circuit test. As a result, it has the potential to minimize any damage to the electrical machine, both the rotor and winding overhang. The DC decay test allows the machine to be tested with no consequences and produces results of sufficient quality to determine the equivalent diagram of synchronous machines.

Future measurement campaigns on high-power synchronous machines should be conducted to expand the comparative range of both methods and further clarify the equivalence range of the two measurement methods.

ACKNOWLEDGMENT

The authors would like to thank engineer Tino Wymann of the Department of Electric Engineering, EPFL, for his valuable contributions to the laboratory experiments conducted as part of the work presented (especially the measurements of the equivalent diagram via other methods). His technical skills in instrumentation, creativity in finding practical solutions, flexibility, and interpersonal skills have been of great importance in this context and are highly appreciated.

REFERENCES

[1] I. Canay, "Determination of model parameters of synchronous machines," *IEE Proc. B, Electr. Power Appl.*, vol. 130, no. 2, pp. 86–94, 1983.

[2] B. Zaker, G. B. Gharehpetian, and M. Karrari, "Improving synchronous generator parameters estimation using *d*–*q* axes tests and considering saturation effect," *IEEE Trans. Ind. Informat.*, vol. 14, no. 5, pp. 1898–1908, May 2018.

[3] E. d. C. Bortoni, B. T. de Araujo, and J. A. Jardini, "Estimation of quadrature axis synchronous reactance using the constant excitation test," *IEEE Power Energy Technol. Syst. J.*, vol. 3, no. 2, pp. 43–50, Jun. 2016.

[4] M. Micev, M. Calasan, D. S. Petrovic, Z. M. Ali, N. V. Quynh, and S. H. E. Aleem, "Field current waveform-based method for estimation of synchronous generator parameters using adaptive black widow optimization algorithm," *IEEE Access*, vol. 8, pp. 207537–207550, 2020.

[5] A. Mitra, A. Mohapatra, S. Chakrabarti, and S. Sarkar, "Online measurement based joint parameter estimation of synchronous generator and exciter," *IEEE Trans. Energy Convers.*, vol. 36, no. 2, pp. 820–830, Jun. 2021.

[6] E. F. Alves, J. K. Nøland, G. Marafioti, and G. Mathisen, "Online parameter identification of synchronous machines using Kalman filter and recursive least squares," in *Proc. 45th Annu. Conf. IEEE Ind. Electron. Soc.*, vol. 1, Oct. 2019, pp. 7121–7128.

[7] Y. Ma, J. Wang, Y. Xiao, L. Zhou, and Z. Q. Zhu, "Two-level surrogate-assisted transient parameters design optimization of a wound-field synchronous machine," *IEEE Trans. Energy Convers.*, vol. 37, no. 1, pp. 737–747, Mar. 2022.

[8] *IEEE Guide for Test Procedures for Synchronous Machines Including Acceptance and Performance Testing and Parameter Determination for Dynamic Analysis*, IEEE Standard 115-2019 (Revision of IEEE Std. 115-2009, 2020, pp. 1–246.

[9] *Rotating Electrical Machines. Part 4: Methods for Determining Synchronous Machine Quantities From Tests*, Int. Electrotechnical Commission (IEC), Standard 60034, 2018.

[10] E. S. Boje, J. C. Balda, R. G. Harley, and R. C. Beck, "Time-domain identification of synchronous machine parameters from simple standstill tests," *IEEE Trans. Energy Convers.*, vol. 5, no. 1, pp. 164–175, Mar. 1990.

[11] M. Arjona, M. Cisneros-Gonzalez, and C. Hernandez, "Development of a synchronous-generator experimental bench for standstill time-domain tests," *J. Appl. Res. Tech.*, vol. 9, no. 2, pp. 117–128, 2011.

[12] F. Sellschopp and M. Arjona, "DC decay test for estimating d-axis synchronous machine parameters: A two-transfer-function approach," *IEE Proc.-Electr. Power Appl.*, vol. 153, no. 1, pp. 123–128, 2006.

[13] M. Vahedi, A. Hassannia, and H. Lotfian, "Unique solution for dynamic parameters identification of a synchronous machine using DC decay test," *J. Electr. Eng.*, vol. 13, no. 3, p. 8, 2013.

[14] M. Cisneros-Gonzalez, C. Hernandez, R. Escarela-Perez, and M. A. Arjona, "Determination of equivalent-circuit parameters of a synchronous generator based on the standstill DC decay test and a hybrid optimization method," *Electric Power Compon. Syst.*, vol. 39, no. 7, pp. 645–659, Apr. 2011.

[15] T. Kano, Y. Watanabe, T. Ara, and T. Matsumura, "Calculation of equivalent circuit constants of synchronous machines considering field transient characteristics using DC decay testing method with open and shorted field windings," *Electr. Eng. Jpn.*, vol. 178, no. 2, pp. 39–46, Jan. 2012.

[16] P. J. Turner, A. B. J. Reece, and D. C. Macdonald, "The DC decay test for determining synchronous machine parameters: Measurement and simulation," *IEEE Trans. Energy Convers.*, vol. 4, no. 4, pp. 616–623, 1989.

[17] L. Majka and D. Szuster, "Application of the stationary DC decay test to industrial turbogenerator model parameter estimation," *Przeglkad Elektrotechniczny*, vol. 90, no. 4, pp. 242–245, 2014.

[18] M. Hasni, O. Touhami, R. Ibtiouen, M. Fadel, and S. Caux, "Synchronous machine parameter identification by various excitation signals," *Electr. Eng.*, vol. 90, no. 3, pp. 219–228, Feb. 2008.

[19] F. Maurer, M. T. Xuan, and J.-J. Simond, "Two novel methods for parameter identification of synchronous machine using DC-decay test with rotor in arbitrary position," in *Proc. 22nd Int. Conf. Electr. Mach. (ICEM)*, Sep. 2016, pp. 633–639.

[20] F. Maurer, M. T. Xuan, and J.-J. Simond, "Two full parameter identification methods for synchronous machine applying DC-decay tests for a rotor in arbitrary position," *IEEE Trans. Ind. Appl.*, vol. 53, no. 4, pp. 3505–3518, Jul. 2017.

[21] Y. Ma, L. Zhou, and J. Wang, "Standstill time-domain response parameter estimation of the large synchronous condenser in arbitrary rotor position," *IEEE Access*, vol. 8, pp. 166047–166059, 2020.

[22] A. Belqorchi, U. Karaagac, J. Mahseredjian, and I. Kamwa, "Standstill frequency response test and validation of a large hydrogenerator," *IEEE Trans. Power Syst.*, vol. 34, no. 3, pp. 2261–2269, May 2019.

[23] L. Vicol, M. Tu Xuan, R. Wetter, J.-J. Simond, and I. A. Viorel, "On the identification of the synchronous machine parameters using standstill DC decay test," in *Proc. 17th Int. Conf. Electr. Mach. (ICEM)*, Sep. 2006, pp. 229.1–229.5.

[24] F. M. Maurer, "Determination of the parameters of a synchronous machine using dc-decay tests," M.Sc. dissertation, EPFL Lausanne, Lausanne, Switzerland, 2009.

[25] P. C. O. Silva, "Modal analysis applied to the stability study of hydroelectric systems with modular structures," Ph.D. dissertation, EPFL, Lausanne, Switzerland, 2015.

[26] I. Canay, "Causes of discrepancies on calculation of rotor quantities and exact equivalent diagrams of the synchronous machine," *IEEE Trans. Power App. Syst.*, vol. PAS-88, no. 7, pp. 1114–1120, Jul. 1969.

[27] F. Maurer, T. L. Toftevaag, and J. K. Nøland, "An analytical prediction model of balanced and unbalanced faults in doubly fed induction machines," *IEEE Trans. Ind. Electron.*, vol. 70, no. 1, pp. 189–199, Jan. 2023.

[28] T. Wymann, "Couplage SIMSEN d'un régulateur de tension," M.Sc. thesis, EPFL, Lausanne, Switzerland, 2008.

[29] J. P. Martin, C. E. Tindall, and D. J. Morrow, "Synchronous machine parameter determination using the sudden short-circuit axis currents," *IEEE Trans. Energy Convers.*, vol. 14, no. 3, pp. 454–459, 1999.

[30] C. E. Tindall, J. P. Martin, D. J. Morrow, and P. A. J. Calvert, "Transient characteristics of small salient-pole alternators," *IEEE Trans. Energy Convers.*, vol. 11, no. 3, pp. 539–546, 1996.

FREDERIC MAURER received the M.Sc. and Ph.D. degrees from the Swiss Federal Institute of Technology at Lausanne (EPFL) in 2009 and 2019, respectively. Since April 2009, he was with Alstom Hydro (now GE Hydro) in different positions, such as a Research and Development Engineer of the Generator Technology Center, a Lead Electrical Engineer, and the Technical Project Manager. Since February 2021, he has been a Guest Researcher with the Department of Electric Power Engineering, Norwegian University of Science and Technology. His current research interests include circulating current, electromagnetics, improved utilization of electrical machines, and electricity market design. He regularly serves as a reviewer for IEEE journals and conferences.

THOMAS ØYVANG (Member, IEEE) received the Ph.D. degree in process, energy, and automation from the University of South-Eastern Norway (USN) in 2018. Since January 2019, he has been an Associate Professor and the Research and Development Manager with the Research Group Electrical Power Systems (EPS), USN, Porsgrunn. He is currently the Project Manager of the Project "System Optimization between power producer and grid owners for more efficient system services (SysOpt)" supported by the Research Council of Norway. His current research interests include control systems, salient-pole synchronous generators, and power system dynamics. He is a Board Member of the Norwegian Academic Committee of Publication in Technology.

JONAS KRISTIANSEN NØLAND (Senior Member, IEEE) was born in Drammen, Norway, in 1988. He received the M.Sc. degree in electric power engineering from the Chalmers University of Technology, Gothenburg, Sweden, in 2013, and the Ph.D. degree in engineering physics from Uppsala University, Uppsala, Sweden, in 2017. Since 2018, he has been an Associate Professor with the Department of Electric Energy, Norwegian University of Science and Technology. He is currently an Associate Professor II with the Department of Electrical Engineering, Information Technology, and Cybernetics, University of South-Eastern Norway (USN), and the Communication Manager of the Hydropower Systems Project SysOpt supported by the Research Council of Norway (RCN). His current research interests include excitation systems, hydro generators, large AC machines, and enhancing their utilization. He has been the Chair of the IEEE Power and Energy Society (PES) Norwegian Chapter since 2022. He serves as an Associate Editor for the IEEE TRANSACTIONS ON ENERGY CONVERSION and the IEEE TRANSACTIONS ON INDUSTRIAL ELECTRONICS.